Progress In Electromagnetics Research C, Vol. 106, 215–228, 2020

Modeling Magnetic Minerals Effect on Water Content Estimation in Porous Media

Tairone P. Leão

Abstract—Magnetic materials are found naturally in certain terrestrial and extra-terrestrial geological settings and can influence subsurface mapping and fluid transport and content estimations. With the advent of magnetic nanoparticle research, there is also the possibility that these will be inputted in the environment on purpose, as research and industrial applications, or inadvertently as contaminants. The presence of magnetic materials is usually not considered in electromagnetic response modeling of saturated or partially saturated porous materials. This is because relative magnetic permeability of most natural materials is close to one, and thus should not affect propagation velocity calculations. The objective of this study was to investigate the effect of magnetic mineral inclusions on the velocity of propagation of an electromagnetic signal on porous materials saturated with water and its influence on volumetric water content estimation. The effective relative dielectric permittivity and magnetic permeability terms were modeled using Maxwell-Garnett, Polder-van Santen, Lichtenecker and Looyenga effective medium approximation equations. Data from three nonmagnetic soils saturated with water to varying degrees were used for preliminary model evaluations. The effect of magnetic minerals was tested by mixing magnetic sand with quartz sand at different proportions and measuring propagation velocity under fully water saturated conditions using Time Domain Reflectometry (TDR). Propagation velocity decreased with increasing magnetic volume fraction, while the effect of increasing magnetic fraction on attenuation factor was not markedly distinct. Water content estimations using models not accounting for magnetic inclusion substantially overestimated volumetric water content in saturated porous media.

1. INTRODUCTION

Subsurface survey and mapping, and fluid content estimation in porous media have applications in geology, geophysics, soil science, engineering, forensics, planetary exploration, agriculture, and environmental sciences. Although the theory related to propagation velocity of an electromagnetic pulse in a porous material partially saturated with gas and liquid is somewhat mature, the influence of magnetic materials on the propagation velocity is often neglected as common natural materials have a relative magnetic permeability very close to one. This implies that the variability on the signal propagation parameters could be related to the electric component, the relative electric permittivity, alone. The effect of magnetic minerals on the estimation of hydrological and geological properties of porous materials using electromagnetic methods is likely to become important over the next decades due to four major factors: i) the need for an increase in water content monitoring and shallow subsurface mapping using electromagnetic methods in soils which under specific geochemical weathering conditions tend to concentrate magnetic minerals such as magnetite and maghemite [1, 2], ii) the input of magnetic nanoparticles [3, 4] on the environment which are a byproduct of industrial, medical and research applications [5] and can be concentrated on the surface of porous materials or

Received 14 August 2020, Accepted 27 October 2020, Scheduled 2 November 2020
* Corresponding author: Tairone Paiva Leão (tleao@unb.br).
The author is with the Faculty of Agronomy and Veterinary Medicine, University of Brasilia, Brasilia, Brazil.

be transported as dispersed phase, with the possibility of concentrating in subsurface materials via aggregation and coagulation processes [6], iii) the use of geophysical methods to assess anthropogenic metal environmental contamination ([2, 7, 8]), and iv) the need of development of methods and devices for exploration of extraterrestrial environments, which can have a high concentration of magnetic minerals such as some Martian environments [9, 10]. The objective of this study was to investigate the effect of magnetic material inclusions on the velocity of propagation of an electromagnetic signal on a multiphase porous material saturated with liquid and its influence on volumetric water content estimation.

2. THEORY

Considering a homogeneous linear media without free charges or free magnetic poles, Maxwell equations can be written as [11]:

$$\nabla \cdot \mathbf{E} = 0, \qquad \nabla \times \mathbf{E} = -\mu^* \frac{\partial \mathbf{H}}{\partial t} \tag{1}$$

$$\nabla \cdot \mathbf{H} = 0, \qquad \nabla \times \mathbf{H} = \epsilon^* \frac{\partial \mathbf{E}}{\partial t} \tag{2}$$

Assuming the field vectors $\mathbf{E}$ and $\mathbf{H}$ as a function of x and t only in Eqs. (1) and (2) results in the set of differential equations:

$$\frac{\partial^2 \mathbf{E}}{\partial x^2} = \epsilon^* \mu^* \frac{\partial^2 \mathbf{E}}{\partial t^2} \tag{3}$$

$$\frac{\partial^2 \mathbf{H}}{\partial x^2} = \epsilon^* \mu^* \frac{\partial^2 \mathbf{H}}{\partial t^2} \tag{4}$$

in which ϵ^* and μ^* are the complex electric permittivity and magnetic permeability, respectively [11, 12]:

$$\epsilon^* = \epsilon' + j\epsilon'' \tag{5}$$

$$\mu^* = \mu' + j\mu'' \tag{6}$$

with $j = \sqrt{-1}$ being the imaginary number. The complex component indicates that both quantities are subject to relaxation phenomena, being composed of an in-phase component, the real component, and out of phase component, the imaginary component. The ratio of the imaginary to the real component is the loss tangent and is a measure of power loss related to the electric and magnetic components:

$$\begin{aligned} \tan \delta_e &= \frac{\epsilon''}{\epsilon'} \\ \tan \delta_m &= \frac{\mu''}{\mu'} \end{aligned} \tag{7}$$

The solution to Eqs. (3) and (4) is a sinusoidal plane wave of angular frequency ω advancing in the direction x with complex propagation factor:

$$\gamma = j\omega\sqrt{\epsilon^*\mu^*} = \alpha + j\beta \tag{8}$$

where α is the attenuation factor, and β is the phase factor of the wave. The phase velocity is then:

$$\frac{dx}{dt} = v = \frac{\omega}{\beta} \tag{9}$$

For an electrical and magnetic loss free, unbounded medium, the imaginary components in Eqs. (5) and (6) can be neglected, i.e., $\epsilon^* = \epsilon'$ and $\mu^* = \mu'$, and by combining Eqs. (5), (6), (8) and (9), the wave group propagation velocity is [11]:

$$v = \frac{1}{\sqrt{\mu'\epsilon'}} = \frac{c}{\sqrt{\mu'_r \epsilon'_r}} \tag{10}$$

in which we can now define μ' as the real component of magnetic permeability in $\mathrm{H\,m^{-1}}$, ϵ' as the real component of electric permittivity of the media in $\mathrm{F\,m^{-1}}$, and μ'_r and ϵ'_r as the real components of relative

magnetic permeability and permittivity of the media, i.e., μ'/μ'_0 and ϵ'/ϵ'_0, which are dimensionless and understood to be equal to or greater than one for the permittivity, and could be greater or less than one for the permeability.

Maxwell equations for a wave propagating in vacuum differ from Eqs. (1) and (2) only in that the permittivity and permeability of vacuum, μ_0 and ϵ_0, are used instead of μ and ϵ, and thus the propagating speed of an electromagnetic wave in vacuum is the speed of light:

$$c = \frac{1}{\sqrt{\mu_0 \epsilon_0}} = \frac{1}{\sqrt{\left(4\pi \times 10^{-7}\,\mathrm{H\,m^{-1}}\right)\left(8.85 \times 10^{-12}\,\mathrm{F\,m^{-1}}\right)}} \qquad (11)$$
$$c \approx 2.9987 \times 10^{8}\,\mathrm{m\,s^{-1}}$$

If the magnetic permeability of the material is very close to the permeability of vacuum, i.e., $\mu \approx \mu_0$ so that $\mu/\mu_0 \approx 1$, the propagation velocity of an electromagnetic wave can be written as:

$$v = \frac{1}{\sqrt{\epsilon'}} = \frac{c}{\sqrt{\epsilon'_r}} \qquad (12)$$

Equation (12) has often been used in geophysical methods for determination of water content and composition in porous media, and transitions in stratified subsurface materials. Methods such as Time Domain Reflectometry (TDR) [13] frequently used in water content estimation in porous materials, and Ground Penetration Radar (GPR) [14] used for subsurface mapping and potentially water content determination, rely on propagation velocity measurements for various calculations. However, for electromagnetic lossy and/or dispersive media, such as materials with high electrical conductivity and for materials containing natural ferrimagnetic minerals, such as those found in soils and weathered rocks derived from mafic and ultramafic rocks, this approximation might be problematic. In these conditions the assumptions that $\epsilon' \gg \epsilon''$ and $\mu' \gg \mu''$ such that $\tan\delta \ll 1$ or $\mu \approx \mu_0$ and $\mu/\mu_0 \approx 1$ might not hold. Now the complex product $\epsilon^*\mu^*$ must be taken into account in electromagnetic wave velocity calculation. From Eqs. (8) and (9) and using complex number algebra it is possible to define the propagation velocity, v and the attenuation coefficient, α [10, 11, 15]:

$$v = \frac{\sqrt{2}c}{\sqrt{(\mu'^2 + \mu''^2)^{1/2}(\epsilon'^2 + \epsilon''^2)^{1/2} + \epsilon'\mu' - \epsilon''\mu''}} \qquad (13)$$

$$\alpha = \frac{\omega}{\sqrt{2}c}\sqrt{(\mu'^2 + \mu''^2)^{1/2}(\epsilon'^2 + \epsilon''^2)^{1/2} - \epsilon'\mu' + \epsilon''\mu''} \qquad (14)$$

which under ideal lossless conditions and $\mu'_r \approx 1$ reduces to Eq. (12) and $\alpha = 0$ as expected. For TDR devices, the attenuation coefficient can be calculated from measured transmitted, reflected and incident amplitudes (or voltages), namely V_t, V_r, and V_0, following [16]:

$$\alpha_D = -\frac{1}{2L}\ln\left[\frac{V_r}{V_t}\right] \qquad (15)$$

or alternatively [17]:

$$\alpha_M = \frac{1}{2L}\ln\left[\frac{V_t(2V_0 - V_t)}{V_0(V_r - V_t)}\right] \qquad (16)$$

Following [11, 18] the complex index of refraction, n^*, can be defined as:

$$n^* = \sqrt{\epsilon^*_r \mu^*_r} \qquad (17)$$

or

$$n^{*2} = \epsilon^*_r \mu^*_r \qquad (18)$$

Representing n^{*2} as κ for simplicity, it is possible to use effective medium approximations (EMA) for estimating the effective electromagnetic approximations of multiphase porous materials. Since most realistic natural porous materials are usually composed of a solid matrix with a porous space filled with varying amounts of liquid and gaseous phases, the mixing models concerned here are those for three or

more interacting phases. Three general EMA are considered. The first is the Polder-van Santen model for random inclusions [19] in a similar form to that presented by [20]:

$$\kappa_{eff} = \kappa_0 + \frac{\frac{1}{3}\sum_{i=1}^{n} f_i(\kappa_i - \kappa_0) \sum_{j=a,b,c} \frac{\kappa_0}{\kappa_0 + N_{ij}(\kappa_i + \kappa_0)}}{1 - \frac{1}{3}\sum_{i=1}^{n} f_i(\kappa_i - \kappa_0) \sum_{j=a,b,c} \frac{N_{ij}}{\kappa_0 + N_{ij}(\kappa_i + \kappa_0)}} \tag{19}$$

where κ_{eff} is the effective squared refractive index for the media, and N_{ia}, N_{ib}, and N_{ic} are geometric factors for the ith phase scatterers, with a, b, and c corresponding to the geometry of the scattering phase, i.e., for spheres $N_a = N_b = N_c = 1/3$, for cylinders (referred to as needles by Sihvola & Kong [20], p.26) $N_a = 0$, $N_b = 1/2$ and $N_c = 1/2$, and for disks $N_a = 1$, $N_b = 0$ and $N_c = 0$, with $N_a + N_b + N_c \equiv 1$ [18]. For spherical scatterers, the formula reduces to a Maxwell-Garnett type equation:

$$\kappa_{eff} = \kappa_0 + \frac{\sum_{i=1}^{n} f_i(\kappa_i - \kappa_0)\frac{3\kappa_0}{\kappa_i + 2\kappa_0}}{1 - \sum_{i=1}^{n} f_i \frac{\kappa_i - \kappa_0}{\kappa_i + 2\kappa_0}} \tag{20}$$

where $f_i = n_i v_i$ is the fractional volume of the ith scatterer.

The second equation considered is the Lichtenecker equation [21, 22]:

$$\kappa_{eff}^{0.5} = \sum_{i=1}^{n} f_i \kappa_i^{0.5} \tag{21}$$

which for a three-phase porous material with pores filled with varying volumes of air a liquid can be written as:

$$\kappa_{eff}^{0.5} = \theta\kappa_l^{0.5} + (1 - \phi)\kappa_s^{0.5} + (\phi - \theta)\kappa_g^{0.5} \tag{22}$$

where the subscripts l, s, and g stand for liquid, solid, and gas; θ is the volumetric water content $[L^3\ L^{-3}]$ (referred to in the context of this study as volumetric water fraction); and ϕ is the total pore volume $[L^3\ L^{-3}]$. Bound water effects were not considered in this case since they are material specific and highly dependent on mineralogy and grain size distribution.

A cubic averaging model was developed independently by Landau and Lifshitz [18] and Looyenga [23], as described in [24], which for a multiphase media can be represented as:

$$\kappa_{eff}^{\frac{1}{3}} = \sum_{i=1}^{n} f_i \kappa_i^{\frac{1}{3}} \tag{23}$$

and expanded in a similar fashion as Eq. (22). EMA equations found in the literature for the effective relative permittivity, ϵ_{eff}, estimation in granular materials are special cases of the equations listed above for when $\epsilon_r' \gg \epsilon_r''$ and $\mu_r' \gg \mu_r''$ with $\mu_r' \approx 1$, following the discussion regarding Eqs. (8), (10) ad (12).

3. MATERIALS AND METHODS

The analysis presented in this study was divided in two stages. The first was to test the EMA (Eqs. (19) to (23)) for the estimation of the effective permittivity of partially saturated media. At this stage data from three nonmagnetic soils of varying mineralogy and grain size distribution were used to evaluate the best approximation for real soils. The soils were a material rich in iron and aluminum oxides, in the form of hematite (α-Fe_2O_3), goethite (α-FeO(OH)), and gibbsite (γ-$Al(OH)_3$) as well as the 1 : 1 layer phyllosilicate mineral kaolinite ($Al_2Si_2O_5(OH)_4$), composed of $823\,g\,kg^{-1}$ clay fraction ($< 2\,\mu m$) (oxidic soil); a soil material rich in gibbsite ($Al(OH)_3$), kaolinite, and 2 : 1 layer phyllosilicates, mainly illite ((K, H_3O)$Al_2Si_3AlO_{10}(OH)_2$) and vermiculite ($(Mg,Fe,Al)_3((Al,Si)_4O_{10})(OH)_2 \cdot 4H_2O$), composed of $746\,g\,kg^{-1}$ clay (clay soil), and a coarse grained quartz (SiO_2) rich soil material with $849\,g\,kg^{-1}$

sand fraction (0.05–2.00 mm) (sandy soil). Nonmagnetic soils data are part of an ongoing study on electromagnetic response of oxidic soils, and details of the soils and experiments can be found in [25].

The second was to test the EMA (Eqs. (19) to (23)) using media created by mixing commercial construction sand and naturally occurring magnetic sand. Magnetic riverbed sand was purchased from a commercial seller. The riverbed sand was collected at the Mococa river in the northern coast of Sao Paulo, Brazil. Heavy minerals found in the region originate from syntectonic granitoids, diorites, gabros, gnaisses, and granulites from the coastal complex [26]. Strongly magnetic minerals were manually separated using a strong $5 \times 5 \times 2.5$ cm neodymium magnet. A fraction of the magnetic separate was ground to a fine powder and subjected to x-ray diffraction (XRD) analysis. Another sample was used for physical characterization including particle density (ρ_{mag}) using the alcohol displacement method, and grain size distribution by the sieve method. Commercial construction sand was sieved to 2 mm and mixed with the magnetic minerals to mass basis proportions of 0% (nonmagnetic minerals only), 5%, 15%, 20%, 25% and 100% (magnetic minerals only). The mixtures were packed onto PVC tubes with average diameter of 4.80 ± 0.03 cm and average height of 16.21 ± 0.02 cm. Because of the large differences of particle density between the magnetic and nonmagnetic materials, resulting bulk density was measured after the experiments. The tubes were then slowly saturated from the bottom up with distilled water. Measurements were performed with the tubes still submerged in order to promote full saturation of the pore space with distilled water. Water temperature was 24.5 °C throughout the experiments.

Electromagnetic wave propagation velocity measurements and trace acquisition were performed using a commercial Time Domain Reflectometer (TDR) manufactured and sold for the water content monitoring market. The system generates a 14 µs 250 mV pulse with an output impedance of $50\,\Omega \pm 1\%$ with operating frequency band centered around 6.25 GHz (Campbell Scientific Ltd.). The signal propagates into a 15-m RG-58 coaxial cable ending in a probe with three rods of 15.00 ± 0.01 mm in length and 3.18 ± 0.01 mm in diameter. The probe is inserted into the material under test. The waveforms were collected and exported as **.dat* files which were then used to extract electromagnetic parameters in worksheet and data analysis software. The propagation velocity was estimated from the waveforms following [27]. Two equations were tested for volumetric water fraction estimation:

$$\theta = 4.3 \times 10^{-6}\epsilon_{eff}^3 - 5.5 \times 10^{-4}\epsilon_{eff}^2 + 2.92 \times 10^{-2}\epsilon_{eff} - 5.3 \times 10^{-2} \tag{24}$$

$$\theta = 0.115\sqrt{\epsilon_{eff}} - 0.176 \tag{25}$$

where θ is the volumetric water fraction $L^3\ L^{-3}$. Eq. (24) is known as Topp's equation [28], and Eq. (25) is the linear square root equation [29]. Both were developed for nonmagnetic materials, and thus it is implicit that they are valid for materials with $\mu_r \approx 1$. Calibration of these equations is also almost always based on the assumption that the imaginary components are negligible, and thus they rely on the assumption that the propagation velocity measured using TDR is related to the real component of relative dielectric permittivity by Eq. (12).

Instrumental error and repeatability of the TDR system used were evaluated by [25]. The standard deviation of measurements was 0.2 for κ_{eff} and 0.006 ns for one-way propagation velocity, as estimated from 30 repeated measures in water at 25 °C. There was no trend in measured values. Experimental error in volumetric water fraction determination based on the gravimetric method was always less than $0.001\,m^3\,m^{-3}$. Error in volumetric water fraction estimation from κ_{eff} using Eqs. (24) and (25) is always less than $0.006\,m^3\,m^{-3}$ in the range of volumetric water fraction from 0.000 to $1.000\,m^3\,m^{-3}$. Because error in estimates was much less than the magnitude of the variables being measured and because error bars would be hidden by the plot symbols, they were not used in this paper.

4. RESULTS AND DISCUSSION

4.1. Nonmagnetic Media Modeling

Modeling of the nonmagnetic media was performed as a preliminary step to select the best equation among Eqs. (19), (20), (22), and (23) for modeling the magnetic media. Since none of the soils used had magnetic minerals as tested using a strong magnet and by x-ray diffraction [25], κ_{eff} was replaced by ϵ_{eff} in Eqs. (19) to (23). Modeling was performed assuming liquid phase permittivity as $\epsilon_l = 80$,

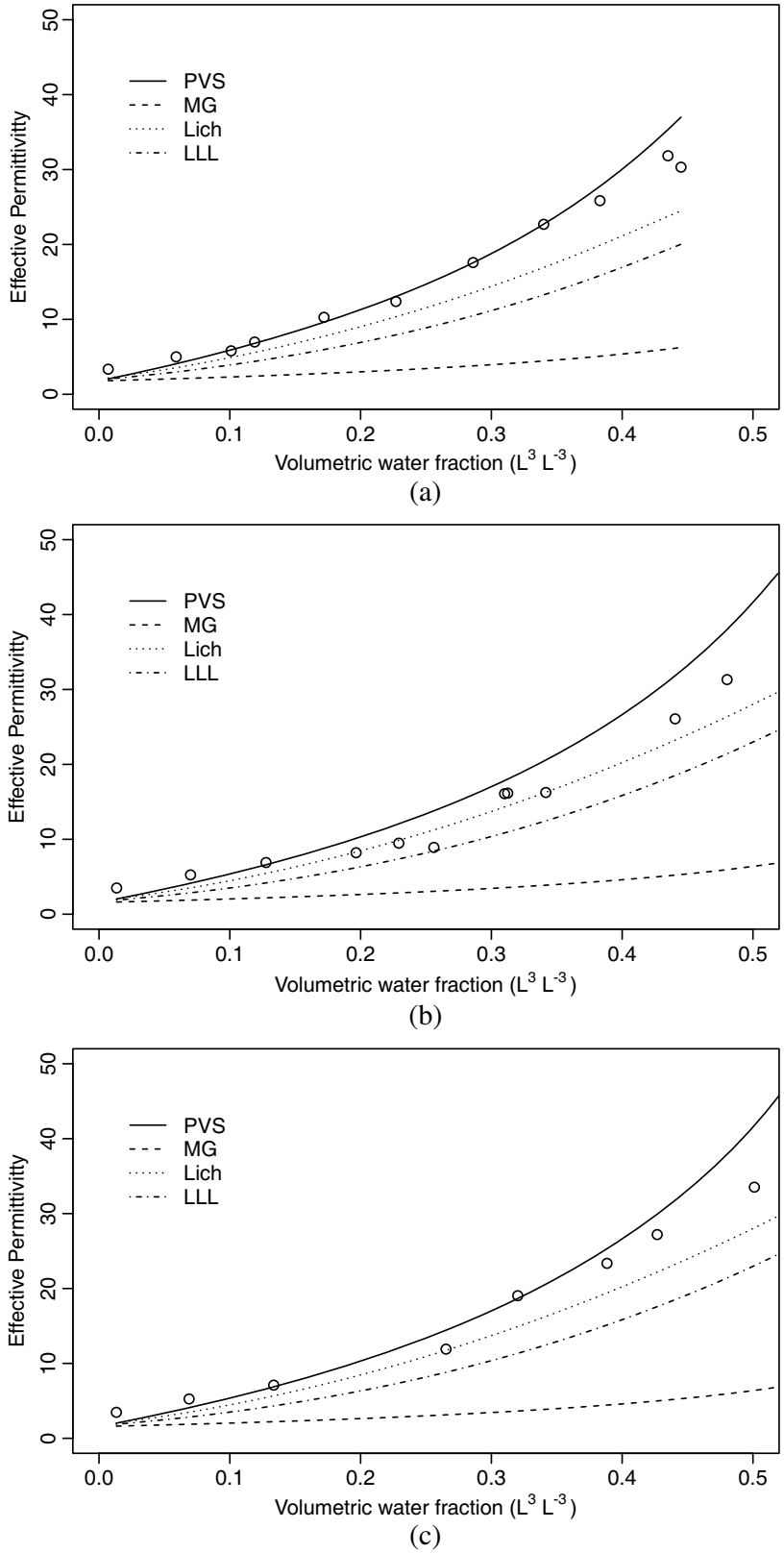

Figure 1. Effective dielectric permittivity vs. volumetric water fraction. (a) Sandy soil. (b) Clay soil. (c) Oxidic soil.

gas as $\epsilon_g = 1$ and solid phase permittivity as $\epsilon_s = 4$ [30]. Effective permittivity for the soil dataset was best described by the Polder-van Santen and Lichtenecker equations (Figure 1). The Polder-van Santen equation (PVS, Eq. (19)) considering solid particles as spheres for the choice of polarizing factors, $N_a = N_b = N_c = 1/3$, and water as needles, $N_a = 0 = N_b = N_c = 1/2$, was particularly effective for estimating volumetric water fractions for the oxidic and the sandy soils, while for the clay soil, observed data were located approximately in between predictions from the Lichtenecker (Lich, Eq. (22)) equation, below, and the PVS equation, above (Figure 1). Choosing water polarizing factors as those of needles did not improve estimates. The Maxwell-Garnett approximation of the PVS equation (MG, Eq. (20)), i.e., $N_a = N_b = N_c = 1/3$ for all phases, performed very poorly compared to the other equations, substantially underestimating effective permittivity of the media. Based on these results, the Landau-Lifshitz-Looyenga (LLL, Eq. (23)), Lichtenecker, and PVS were chosen for modeling the magnetic media.

4.2. Magnetic Media Modeling

X-ray diffraction analysis of the magnetic phase used on the experiments showed presence of magnetite and ilmenite (Figure 2). Although ilmenite is identified as a weakly magnetic paramagnetic mineral, the separation process using a strong magnet concentrated only strongly magnetic phase. Ilmenite particles present are likely transitional phases to magnetite, titanomagnetites and titanohematites, as these minerals have common genesis in mafic rocks and could be either ferromagnetic or present remnant magnetization [31, 32]. Magnetization hysteresis curve obtained using Quantum Designs — Physical Property Measurement System is shown in Figure 3. Hysteresis loop showed little displacement between the saturation and desaturation curves (Figure 3(a)). Relative magnetic permeability at the saturation point was calculated from the constitutive relationships:

$$\mathbf{M} = \chi_m \mathbf{H} \tag{26}$$

and

$$\mu_r = \frac{\mu}{\mu_0} = 1 + \chi_m \tag{27}$$

where χ_m is the dimensionless magnetic susceptibility, and $\mathbf{M}$ and $\mathbf{H}$ are the magnetization and applied magnetic field, both in $\mathrm{A\,m^{-1}}$ [12]. Saturation permeability was $\mu_r = 1.1439$ which is in agreement [33] or slightly lower [10] than natural granular magnetite, but 2 to 4 times below the values reported for various synthetic magnetic mixtures [34, 35]. Lower values observed for natural materials might be related to purity, grain size distribution of the material and frequency of operation. 91.2% of the particles had diameter between 0.050 mm and 0.25 mm with 9.8% between 0.25 mm and 0.5 mm, with minor proportions of finer and coarser materials, average particle density was $\rho_{mag} = 4970 \pm 140\,\mathrm{kg\,m^{-3}}$. The material before magnetic sieving was 78.45% magnetic on mass basis. The nonmagnetic phase was

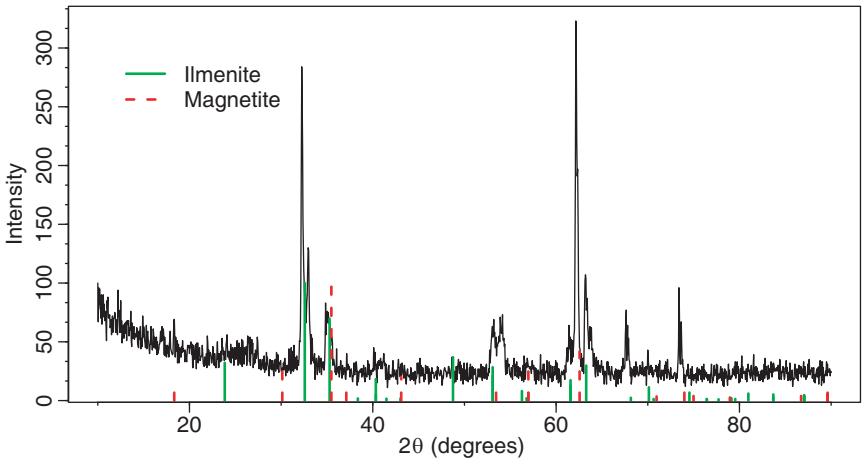

Figure 2. Powder x-ray diffraction of magnetic mineral sample used in the experiments.

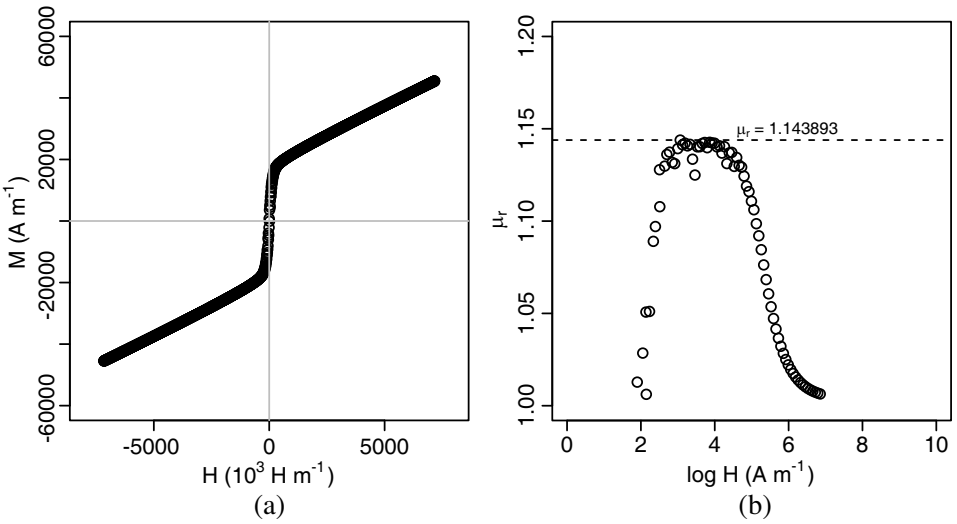

Figure 3. Hysteresis curve for the magnetic sand used in the experiments. (a) Hysteresis loop. (b) Relative magnetic permeability near saturation region.

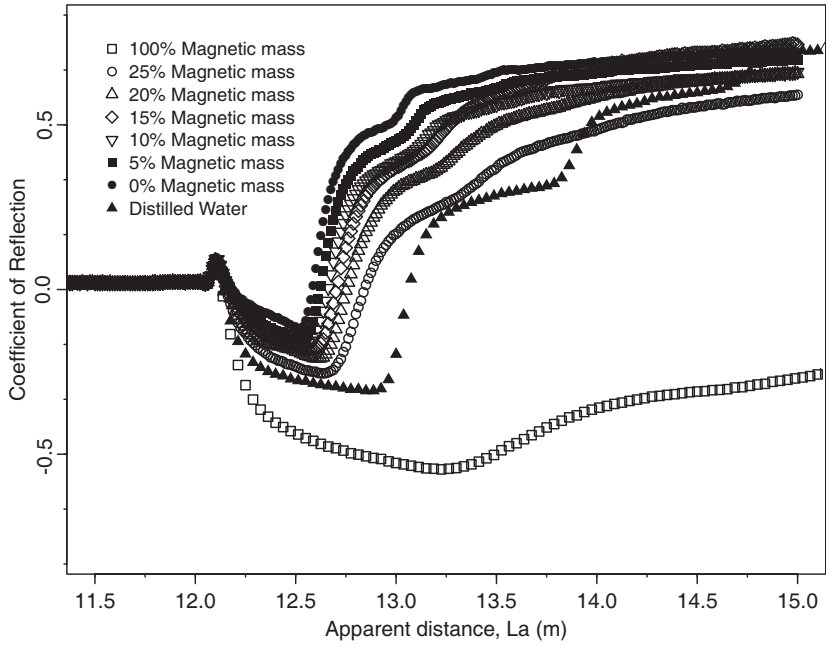

Figure 4. TDR waveform for different mixtures of magnetic and nonmagnetic materials.

mainly composed of quartz sand as evidenced by visual inspection and XRD determined before magnetic sieving.

TDR traces revealed a strong influence of magnetic fraction on apparent distance and travel time, and on the reflection at the end of the probe (Figure 4). The reflection voltage at the end of the probe can be evaluated as the coefficient of reflection value corresponding to the first step after the end of the probe [27]. For distilled water, the step is located around an apparent distance of 13.5 m, while for the distilled water magnetic material only mix, a very subtle step can be found around 14.0 m to 14.5 m. The decrease in reflected voltage is caused by an increase in attenuation and dispersion of the electromagnetic wave by the media with increase in magnetic material content [15, 17]. The choice for water instead of air for pore saturating media allowed for a better distinction between reflections

as opposed to [10, 15, 17] for example, which used air dried samples. The experimental setup used in this study is similar to that of [36], which also indicates that using water as a background medium allows for a better distinction not only of the end of the probe reflection, but of the amplitude of the reflection coefficient within the probe, as identified by the influence of the filling material on coefficient of reflection minima (Figure 4).

Propagation velocity can be related to κ_{eff} by:

$$v = \frac{c}{\sqrt{\kappa_{eff}}} \tag{28}$$

This equation can take forms similar to that of Eqs. (10), (12), or (13) depending on the electromagnetic properties of the media in which the signal is propagating. Assuming for the time being that κ_{eff} is a term where such properties are unknown, it is possible to use wave group propagation velocities calculated from TDR traces (Figure 4) in order to estimate κ_{eff} and use this value on the EMA equations evaluated on the preceding section. It is apparent from Eqs. (19), (22), and (23) that κ_{eff} is some mathematical (and physical) mixture of the terms κ_s, κ_l and κ_{mag}, where l is the liquid phase or distilled water, s the solid phase or construction sand, and mag the magnetic sand. Since distilled water and quartz sand are nonmagnetic and lowly lossy, it was assumed for modeling purposes that $\kappa_s = \epsilon_s$ and $\kappa_l = \epsilon_l = 80$. Observed κ_{eff} calculated from TDR traces was compared to predicted κ_{eff} using $\kappa_s = \epsilon_s$ and κ_{mag} as fitting parameters on the PVS, Lich and LLL equations (Figure 5). The analysis shows that predicted and observed values were in very close agreement ($R^2 > 0.99$) with estimated $\kappa_s = \epsilon_s$ within realistic ranges for quartz sand, i.e., from 2.22 to 6.41. The equations predicted very high κ_{mag}, ranging from 250 to 315 (Figure 5). Combining Eq. (28) with Eq. (13), κ_{mag} must be some function of the individual real and imaginary permittivities and permeabilities of the magnetic media:

$$\kappa_{mag} = \frac{\left(\mu_r'^2 + \mu_r''^2\right)^{1/2}\left(\epsilon_r'^2 + \epsilon_r''^2\right)^{1/2} + \epsilon_r'\mu_r' - \epsilon_r''\mu_r''}{2} \tag{29}$$

Considering for example values of solid phase permittivity for magnetite $\epsilon_r' = 25$ to 27 reported in [37], much higher values for solid phase permeability, on the order of $\mu_r' \approx 10$ and $\mu_r'' \approx 0.5$ would be needed to reach the values of κ_{mag} found in this research. All studies found on the literature in addition to the present study have worked with granular magnetite samples and/or composites, and thus it is likely that solid magnetite will have much higher values than reported. [37] worked to minimize air gaps in samples used for measurements which can significantly decrease permittivity values. [34], for example, found values for synthetic sintered Fe_3O_4 around 10 to 15 for μ_r', and 0.5 to 2.5 for μ_r'', at various frequencies at $\approx 300\,\mathrm{K}$, with powder samples presenting much lower values. In the end, the lack of standardization of frequencies, measuring equipment, sample format (bulk versus powder), and intrinsic physical properties of the materials tested makes estimations of solid phase magnetic permeability from the literature a difficult endeavor. Estimating κ_{mag} from values of [34, 37] would result in values ranging from 250 to 375, within the range of values predicted here. There is also literature evidence that permittivity of bulk magnetite is in fact very high. [38] reported from an indirect source a permittivity value of 100 for bulk magnetite while [39, 40] reported high permittivity values for single crystal magnetites at low temperatures at various frequencies. Considering the discussion above, and from permeability data measured in this study, permittivity and not permeability might be the main control on propagation velocity in porous media rich in magnetic minerals.

From the analysis presented and from Eq. (28), it is possible to conclude that propagation velocity of electromagnetic waves in porous media does follow EMA rules and therefore Eqs. (20), (21) and (23) can be written as:

$$v_{eff} = \left[\frac{1}{v_0^2} + \frac{\dfrac{1}{3}\displaystyle\sum_{i=1}^{n} f_i\left(\frac{1}{v_i^2} - \frac{1}{v_0^2}\right)\sum_{j=a,b,c}\frac{\dfrac{1}{v_0^2}}{\dfrac{1}{v_0^2} + N_{ij}\left(\dfrac{1}{v_i^2} + \dfrac{1}{v_0^2}\right)}}{1 - \dfrac{1}{3}\displaystyle\sum_{i=1}^{n} f_i\left(\frac{1}{v_i^2} - \frac{1}{v_0^2}\right)\sum_{j=a,b,c}\frac{N_{ij}}{\dfrac{1}{v_0^2} + N_{ij}\left(\dfrac{1}{v_i^2} + \dfrac{1}{v_0^2}\right)}}\right]^{-1} \tag{30}$$

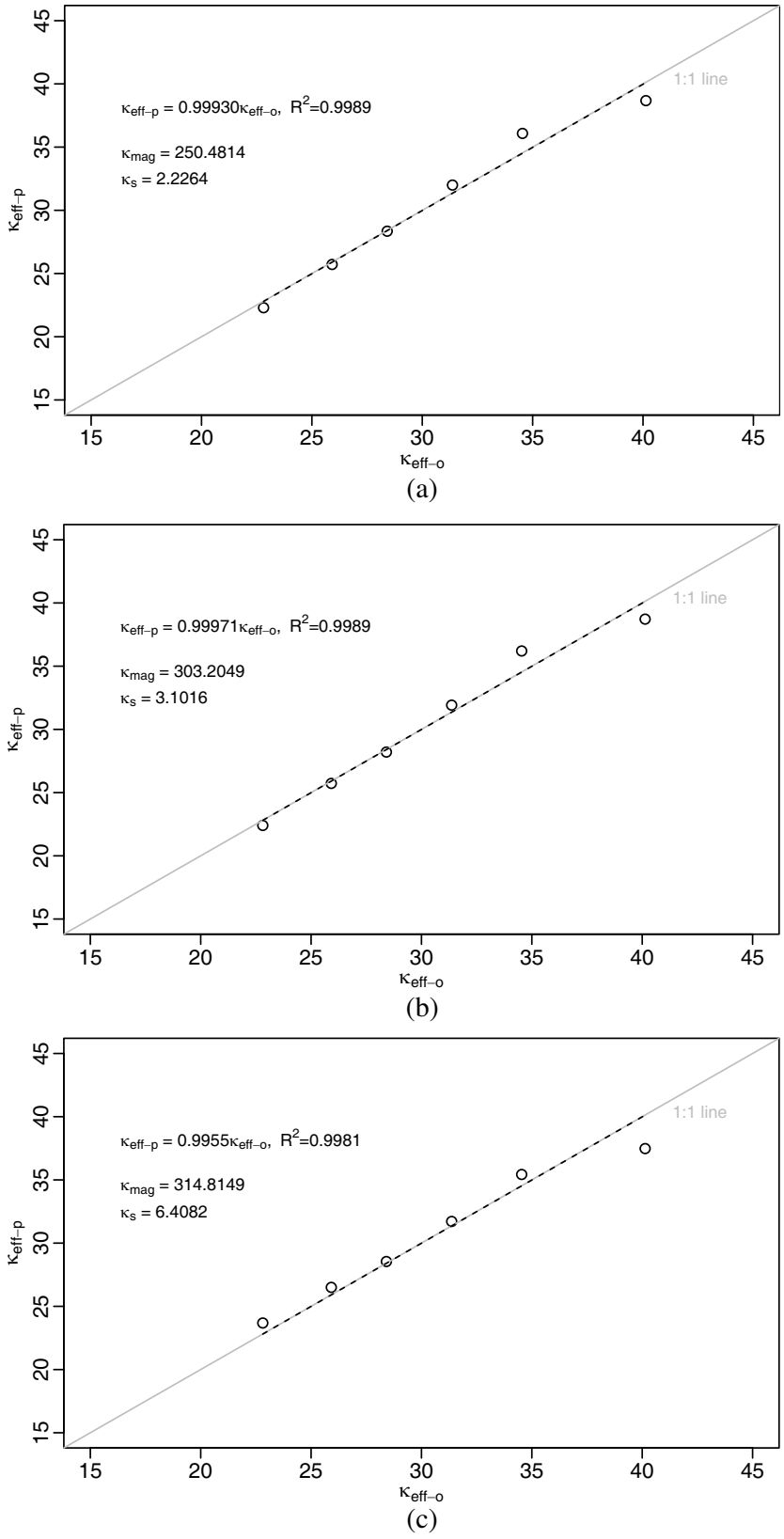

Figure 5. Predicted versus estimated effective relative permittivity. (a) Polder-van Santem equation. (b) Lichtenecker equation. (c) Landau-Lifshitz-Looyenga.

$$v_{eff} = \left[\sum_{i=1}^{n} \frac{f_i}{v_i}\right]^{-1} \tag{31}$$

$$v_{eff} = \left[\sum_{i=1}^{n} \frac{f_i}{v_i^{\frac{2}{3}}}\right]^{-\frac{3}{2}} \tag{32}$$

Figure 6(a) shows observed and predicted propagation velocities using these equations and data from Figure 4 for calculating propagation velocity. Predicted lines were calculated based on a fixed volumetric solid phase fraction of $f_s = 0.6\ L^3\ L^{-3}$ and volumetric water fraction of $\theta = 0.4\ L^3\ L^{-3}$. Propagation velocity on water was calculated assuming $\epsilon_l = 80$. Predictions from Eqs. (30), (31), and (33) were very close to each other and were relatively close to measured data. Deviations from observed data might be related to variations in packing density due to the large differences in particle density between magnetic and nonmagnetic solids. Calculated propagation velocity on solids used on the estimations ranged from 11.8 to 20.1 cm ns^{-1} for quartz and 1.69 to 1.89 cm ns^{-1} for magnetic minerals. Although velocity reduction can be correlated with attenuation of the electromagnetic signal in magnetic media [15, 17] the effects observed here are difficult to differentiate at low magnetic mass fraction (Figure 6(b)). The same issue was reported for TDR attenuation estimations in other research [15, 17]. Data in Figure 6(b) are from Eqs. (15) and (16) used on the TDR traces shown in Figure 4. The relationship between attenuation coefficient and magnetic mass fraction is not clearly defined at lower magnetic fractions. The model of [16] was less sensitive to variations at lower magnetic fractions while the model of [17] showed a slight increase in attenuation at magnetic fractions lower than 40% (Figure 6(b)). At the maximum value of magnetic fraction, 100%, attenuation two to threefold higher than that of nonmagnetic media was observed.

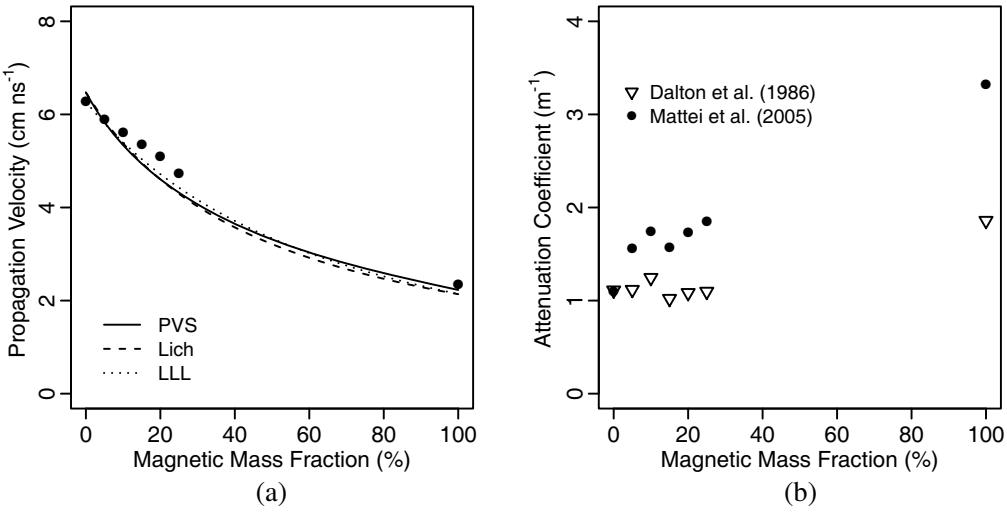

Figure 6. (a) Propagation velocity and (b) attenuation coefficient vs. magnetic mass fractions.

Figure 7 shows predicted and observed volumetric water fractions for the experiments performed in this research. The experiments were planned such that the volumetric water fractions were to remain approximately constant except for variability induced by the inclusion of magnetic minerals which are heavier and have grains sizes and geometries different from that of the quartz sand used. As expected, the observed variability in volumetric water fraction (also known as volumetric water content on the soil science literature) was small (Figure 7). The predictions from Eqs. (24) and (25) on the other hand substantially overestimated volumetric water fraction for κ_{eff} values greater than that of distilled water. For the square root equation the rise was approximately linear, with a predicted volumetric water fraction of $1.2890 \pm 0.0009\ L^3\ L^{-3}$ at the $\approx 100\%$ magnetic solid fraction filled with water, while for the third degree polynomial equation, after κ_{eff} reaches the value of pure water ≈ 80, the predictions

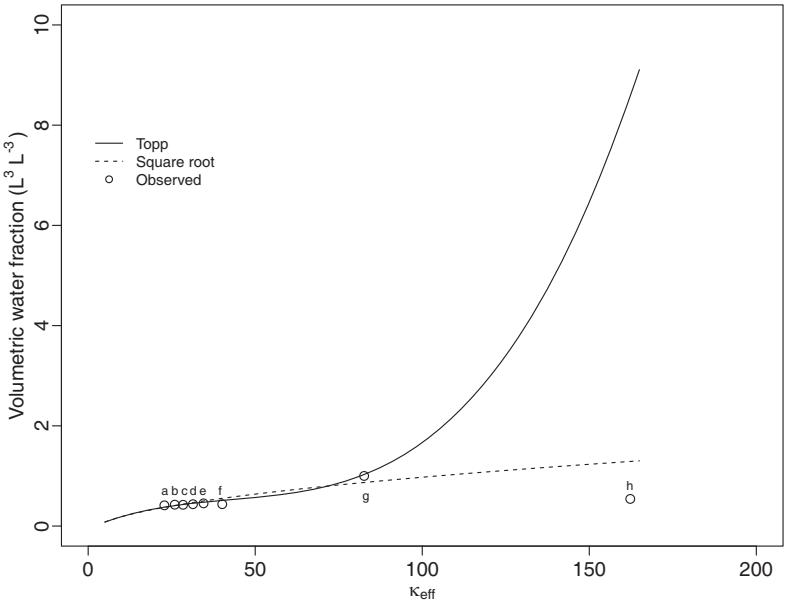

Figure 7. Predicted volumetric water fractions from equations (24, Topp) and (25, Square root) as a function of squared effective index of refraction (κ_{eff}). (a) 0%, (b) 5%, (c) 10%, (d) 15%, (e) 20%, (f) 25%, and (h) $\approx$ 100% magnetic fraction, and (g) is pure distilled-water.

increase in a cubic rate, with values exploding to predicted volumetric water fractions greater than 8.00 ± 0.04 L^3 L^{-3} at $\approx$ 100% magnetic solid fraction. It is important to note that volumetric water fractions greater than pore volume, which is commonly around 0.5 L^3 L^{-3}, are a physical impossibility, highlighting thus the problem with the error induced by the presence of magnetic minerals.

5. CONCLUDING REMARKS

The presence of magnetic heavy minerals can significantly affect effective electromagnetic parameters, and thus propagation velocity in multiphase porous media saturated with water. Modeling results indicate that heavy magnetic minerals appear to have high values of electric permittivity which in turn can cause substantial decrease in propagation velocity. This decrease can lead to erroneous interpretation of GPR parameters in magnetic materials and can lead to major overestimation errors in water content estimation when calibration equations that do not account for the effect of magnetic phase are used. This is particularly important in methods that rely on velocity of propagation for estimating volumetric water content, as is the case with TDR and GPR. Water content overestimation greater than around 10.0 ± 0.2% is to be expected at magnetic fraction contents around 20% to 25% for both water content calibration equations investigated, the overestimation increasing thereafter with magnetic fraction. Based on the above, it is recommended that the effects of magnetic phase are considered when using sensors in environments rich in magnetic minerals. It is also necessary to refine techniques for measuring solid phase relative permittivity and permeability, in order for those to be included in the models. The method used for permeability measurement, grain size, and porosity can substantially influence permeability measurements, which in turn make it difficult to accurately estimate the influence of this parameter on propagation velocity.

ACKNOWLEDGMENT

This work was funded by the Brazilian National Council for Scientific and Technological Development (CNPq) grant 473020/2013-0. I am thankful to the Institutes of Chemistry and Geology of the University of Brasilia for XRD characterization and the Institute of Physics of the University of Brasilia for the magnetic measurements.

REFERENCES

1. Chen, T., H. Xu, Q. Xe, J. Chen, J. Ji, and H. Lu, "Characteristics and genesis of maghemite in Chinese loess and paleosols: Mechanisms for magnetic susceptibility enhancement in paleosols," *Earth Planet. Sci. Lett.*, Vol. 240, 790–802, 2005.
2. Fialova, H., G. Maier, E. Petrovsky, A. Kapieka, T. Boyko, and R. Schloger, "Magnetic properties of soils from sites with different geological and environmental settings," *J. Appl. Geophys.*, Vol. 59, 273–283, 2005.
3. Vatta, L. L., R. D. Sanderson, and K. Koch, "Magnetic nanoparticles: Properties and potential applications," *Pure Appl. Chem.*, Vol. 78, 1793–1801, 2006.
4. Mohammed, L., H. G. Gomaa, D. Ragab, and J. Zhu, "Magnetic nanoparticles for environmental and biomedical applications: A review," *Particuology*, Vol. 30, 1–14, 2017.
5. Akbarzadeh, A., M. Samiei, and S. Davaran, "Magnetic nanoparticles: Preparation, physical properties, and applications in biomedicine," *Nanoscale Res. Lett.*, Vol. 7, 144, 2012.
6. Tang, S. C. N. and I. M. C. Lo, "Magnetic nanoparticles: Essential factors for sustainable environmental applications," *Water Res.*, Vol. 47, 2613–2632, 2013.
7. Chudanicova, M. and S. M. Hutchinson, "Magnetic signature of overbank sediment in industrial impacted floodplains identified by data mining methods," *Geophys. J. Int.*, Vol. 207, 1106–1121, 2016.
8. Wang, G., F. Ren, J. Chen, Y. Liu, F. Ye, F. Oldfield, W. Zhang, and X. Zhang, "Magnetic evidence of anthropogenic dust deposition in urban soils of Shangai, China," *Chem. Erde*, Vol. 77, 421–428, 2017.
9. Picardi, G., et al., "Radar sounding of the subsurface of mars," *Science*, Vol. 310, 1925–1928, 2008.
10. Pettinelli, E., G. Vannaroni, A. Cereti, A. R. Pisani, F. Paolucci, D. Del Vento, D. Dolfi, S. Riccioli, and F. Bella, "Laboratory investigations into electromagnetic properties of magnetite/silica mixtures as Martian soil simulants," *Journal of Geophysical Research*, Vol. 110, E04013, 2005.
11. Von Hippel, A., *Dielectric and Waves*, 284, Wiley, Hoboken, 1954.
12. Griffiths, D. J., *Introduction to Electrodynamics*, 4th Edition, 604, Pearson Education Inc., 2013.
13. Robinson, D. A., S. B. Jones, J. M. Wraith, D. Or, and S. P. Friedman, "Review of advances in dielectric and electrical conductivity measurements using time domain reflectometry," *Vadose Zone J.*, Vol. 2, 444–475, 2003.
14. Huisman, J. A., S. S. Hubbard, J. D. Redman, and A. P. Annan, "Measuring soil water content with ground penetrating radar: A review," *Vadose Zone J.*, Vol. 2, 476–491, 2003.
15. Mattei, E., A. De Santis, A. D. Di Matteo, E. Pettinelli, and G. Vannaroni, "Electromagnetic parameters of dielectric and magnetic mixtures evaluated by time-domain reflectometry," *IEEE Geosci. Remote Sens. Lett.*, Vol. 5, 730–734, 2008.
16. Dalton, F. N. and M. Th. van Genuchten, "The time-domain reflectometry method for measuring soil water content and salinity," *Geoderma*, Vol. 38, 237–250, 1986.
17. Mattei, E., A. De Santis, A. D. Di Matteo, E. Pettinelli, and G. Vannaroni, "Time domain reflectometry of glass beads/magnetite mixtures: A time domain study," *Appl. Phys. Lett.*, Vol. 86, 224102, 2005.
18. Landau, L. D. and E. M. Lifshitz, *Electrodynamics of Continuous Media*, Pergamon Press, 1960.
19. Polder, D. and J. H. Van Santem, "The effective permeability of mixtures of solids," *Physica XII*, Vol. 5, 257–271, 1946.
20. Sihvola, A. H. and J. A. Kong, "Effective permittivity of dielectric mixtures," *IEEE Trans. Geosci. Rem. Sens.*, Vol. 26, 420–429, 1988.
21. Birchak, J. P., G. G. Gardner, J. E. Hipp, and J. M. Victor, "High dielectric constant microwave probes for sensing soil moisture," *Proc. IEEE*, Vol. 62, 93–98, 1974.
22. Zakri, T., J. P. Laurent, and M. Vauclin, "Theoretical evidence for 'Lichtenecker's mixture formulae' based on the effective medium theory," *J. Physics D*, Vol. 31, 1589–1594, 1998.

23. Looyenga, H., "Dielectric constant of homogenous mixtures," *Mol. Phys.*, Vol. 9, 501–511, 1965.
24. Dube, D. C., "Study of Landau-Lifshitz-Looyenga's formula for dielectric correlation between powder and bulk," *J. Phys. D: Appl. Phys.*, Vol. 3, 1648–1652, 1970.
25. Leão, T. P., B. D. C. Freire, V. B. Bufon, and F. F. H. Arágon, "Using Time Domain Reflectometry to estimate water content of three soil orders under savanna in Brazil," *Geoderma Regional.*, Vol. 21, e00280, 2020.
26. Correa, I. C. S. and A. R. D. Elias, "Minerais pesados dos sedimentos do fundo da enseada de Caraguatatuba, São Paulo, Brasil," *Pesquisas em Geociências*, Vol. 28, 37–47, 2001.
27. Noborio, K., "Measurement of soil water content and electrical conductivity by time domain reflectometry: A review," *Comput. Electr. Agricult.*, Vol. 31, 213–237, 2001.
28. Topp, G. C., J. L. Davis, and A. P. Annan, "Electromagnetic determination of soil water content: Measurements in coaxial transmission lines," *Water Resour. Res.*, Vol. 16, 574–582, 1980.
29. Topp, G. C. and W. D. Reynolds, "Time domain reflectometry: A seminal technique for measuring mass and energy in soil," *Soil Till. Res.*, Vol. 47, 125–132, 1998.
30. Robinson, D. A. and S. P. Friedman, "A method for measuring the solid particle permittivity or electrical conductivity of rocks, sediments, and granular materials," *J. Geophys. Res.*, Vol. 108, 2076, 2003.
31. Robinson, P., R. J. Harrison, S. A. McEnroe, and R. B. Hargraves, "Lamellar magnetism in the hematite-ilmenite series as an explanation for strong remanent magnetization," *Nature*, Vol. 418, 517–520, 2002.
32. Ursula, S., L. Dominique, M. Burchard, and R. Engelmann, "The titanomagnetite-ilmenite equilibrium: New experimental data and thermo-oxybarometric application to the crystallization of basic to intermediate rocks," *J. Petrol.*, Vol. 49, 1161–1185, 2008.
33. Van Dam, R. L., J. M. H. Hendrickx, N. J. Cassidy, R. E. North, M. Dogan, and B. Borchers, "Effects of magnetite on high-frequency ground penetrating radar," *Geophysics*, Vol. 78, H1–H11, 2013.
34. Iwauchi, K., Y. Kital, and N. Koizumil, "Magnetic and dielectric properties of Fe_3O_4," *J. Phys. Soc. Jpn.*, Vol. 49, 1328–1335, 1980.
35. Hotta, M., M. Hayashi, A. Nishikata, and K. Nagata, "Complex permittivity and permeability of SiO_2 and Fe_3O_4 powders in microwave frequency range between 0.2 and 13.5 GHz," *ISIJ International*, Vol. 49, 1443–1448, 2009.
36. Robinson, D. A., J. P. Bell, and C. H. Batchelor, "Influence of iron minerals on the determination of soil water content using dielectric techniques," *J. Hydrol.*, Vol. 161, 169–180, 1994.
37. Cassidy, N. J., "Frequency-dependent attenuation and velocity characteristics of nano-to-micro scale, lossy, magnetite-rich materials," *Near Surf. Geophys.*, Vol. 6, 341–354, 2008.
38. Fannin, P. C., C. N. Marin, I. Malaescu, and N. Stefu, "Microwave dielectric properties of magnetite colloidal particles in magnetic fluids," *J. Phys.: Condens. Matter*, Vol. 19, 036104, 2007.
39. Schrettle, F., S. Krohns, P. Lunkenheimer, V. A. M. Brabers, and A. Loidl, "Relaxor ferroelectricity and the freezing of short-range polar order in magnetite," *Phys. Rev. B*, Vol. 83, 195109, 2011.
40. Angst, M., S. Adiga, S. Gorfman, M. Ziolkowski, J. Strempfer, C. Grams, M. Pietsch, and J. Hemberger, "Intrinsic ferroelectricity in charge-ordered magnetite," *Crystals*, Vol. 9, No. 11, 546, 2019.